

Transforming from Kitaev to Disguised Ising Chain: Application to CoNb_2O_6

Derek Churchill¹ and Hae-Young Kee^{1,2,*}

¹*Department of Physics, University of Toronto, Ontario, Canada M5S 1A7*

²*Canadian Institute for Advanced Research, CIFAR Program in Quantum Materials, Toronto, Ontario, Canada, M5G 1M1*

 (Received 28 March 2024; accepted 25 June 2024; published 30 July 2024)

For many years, CoNb_2O_6 has served as an exemplar of the one-dimensional Ising model. However, recent experimental and theoretical analyses challenge its applicability to this material. Prior to that, a tailored spin model for $3d^7$ systems such as Co^{2+} , known as the JKT model, has emerged, featuring Heisenberg (J), Kitaev (K), and Gamma (Γ) interactions. While these interactions are permitted by the symmetry of the system, their role in CoNb_2O_6 remains enigmatic. We present a microscopic theory based on spin-orbit entangled $J_{\text{eff}} = 1/2$ states, aimed at elucidating the roles of Kitaev and Gamma interactions in shaping Ising anisotropy. Leveraging strong coupling theory, we identify a dominant ferromagnetic Kitaev interaction. Furthermore, by comparing dynamical structure factors obtained via exact diagonalization with those from inelastic neutron scattering experiments, we find an antiferromagnetic Γ interaction, which dictates the Ising axis and explains the mechanism behind moment pinning. Our theory provides a microscopic origin for Ising behavior in spin-orbit coupled one-dimensional chains and posits CoNb_2O_6 as a rare Kitaev chain.

DOI: 10.1103/PhysRevLett.133.056703

Introduction—The one-dimensional (1D) transverse field Ising model is one of the simplest models exhibiting a quantum phase transition and quantum critical point. The realization of such materials has posed a formidable challenge, with only a limited number of solid-state materials demonstrating a 1D Ising quantum critical point under a magnetic field. Among the extensively studied 1D Ising systems, CoNb_2O_6 stands out as one of the most investigated examples [1–14].

CoNb_2O_6 exhibits the anticipated quantum critical point under an applied magnetic field of approximately 5 T, as verified through inelastic neutron scattering (INS) [6], specific heat [15], THz spectroscopy [16–19], and nuclear magnetic resonance measurements [20]. The predicted E_g symmetry [21–24], a noteworthy hallmark of the 1D Ising chain near the quantum critical point, has also been identified using INS measurement [6]. However CoNb_2O_6 displays features inconsistent with those for a pure 1D Ising model with quantum motion of domain walls present even in the absence of an applied transverse field [6]. This was recently attributed to a symmetry-allowed staggered spin exchange term [10], and a twisted 1D Kitaev model composed of a bond-dependent Ising interaction was suggested to explain features observed in THz spectroscopy measurements in a low transverse field [18].

Around the same time, the nearest neighbor (n.n.) exchange model of $3d^7$ honeycomb materials was developed [25,26], which is composed of Heisenberg (J),

bond-dependent Kitaev (K), and Gamma (Γ) interactions known as the JKT model [27–38]. Since Co^{2+} exhibits a $3d^7$ configuration in CoNb_2O_6 , the 1D version of the JKT model allowed by the system’s symmetry is expected. However, the mechanism by which the JKT model relates to the Ising anisotropy, their strengths, and the specific roles of each exchange interaction remain unresolved.

Here we present a microscopic theory of the n.n. exchange interactions to elucidate their roles in Ising anisotropy and domain-wall excitations in the ferromagnetic (FM) ordered state. We find that the FM Kitaev interaction is dominant in CoNb_2O_6 . The Ising anisotropy and pinning of the moment direction is due to the antiferromagnetic (AFM) Γ interaction. Contributions from other small interactions generated by the octahedra distortion and dynamical structure factor (DSF) obtained via exact diagonalization (ED) are also presented.

Microscopic Hamiltonian—To derive a microscopic theory, we commence with a brief review of the atomic wave functions of Co^{2+} , which gives rise to $J_{\text{eff}} = 1/2$ states through the interplay of Hund’s coupling and spin-orbit coupling (SOC) [25,26,35]. A Co^{2+} ion with a $3d^7$ electron configuration is surrounded by an octahedral cage of oxygen atoms. This generates a cubic crystal field that splits the d -orbital manifold into t_{2g} and e_g states, separated by the cubic crystal field energy Δ_c . Because of a large Hund’s coupling J_H ($J_H > \Delta_c$), the Co^{2+} ion forms a high-spin $t_{2g}^5 e_g^2$ electron configuration and a 12-fold degenerate $L = 1, S = 3/2$ subspace is further split by SOC resulting in a low-energy, pseudospin-1/2 Kramer’s doublet [25,26].

*Contact author: hy.kee@utoronto.ca

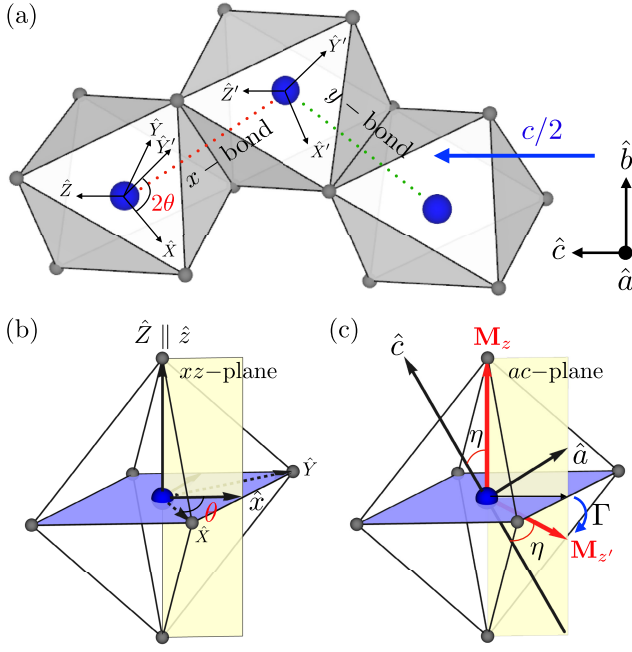


FIG. 1. (a) Twisted chain consisting of an x and y bond. Each site within the unit cell contains local Cartesian coordinates, XYZ vs $X'Y'Z'$ (\hat{X} and \hat{Y}' are chosen along the anion directions), related by a c -glide symmetry along the chain \hat{c} direction. $\hat{Z} \approx \hat{Z}'$ such that the XY and $X'Y'$ plane lie approximately within the same plane, and the angle between the \hat{X} and \hat{Y}' axes is defined by 2θ . For an ideal octahedra chain with $\theta = 45^\circ$, (b) \hat{Z} lies within the ac plane, and the global xyz coordinate is shown with respect to the local XYZ coordinate, and (c) the red arrows \mathbf{M}_z and $\mathbf{M}_{z'}$ in the ac plane represent two magnetic moment directions, where $\eta \sim 35^\circ$ measured from the $\pm\hat{c}$ axis. The anisotropic g factor changes $\eta \sim 33^\circ$ (see the Supplemental Material [39] for the details), closer to the experimental findings, 31° [2,4].

The Co^{2+} ions form a 1D chain in the ac plane where the chain is along the crystallographic c axis as shown in Fig. 1(a). They are linked by distorted edge-sharing oxygen octahedra which define two local Cartesian coordinate systems denoted by XYZ and $X'Y'Z'$, respectively, where the \hat{X} and \hat{Y}' axis are chosen to be along the anion directions and make an angle 2θ . Because of the staggered distortion of the oxygen cages, C_2 symmetries are lost, but a glide symmetry remains with the glide ac plane at $b = 1/4$ as shown in the blue arrow in Fig. 1(a).

We first develop a theory for ideal octahedra cages, with $\hat{X} = \hat{X}'$, $\hat{Y} = \hat{Y}'$, and $\hat{Z} = \hat{Z}'$, and the \hat{Z} axis lying within the ac plane. Using the local XYZ coordinates, the n.n. generic $J_{\text{eff}} = 1/2$ exchange model is given by the $JK\Gamma$ model [25,26,31,36,38]:

$$H_{ij}^0 = [J\mathbf{s}_i \cdot \mathbf{s}_j + Ks_i^x s_j^x + \Gamma(s_i^x s_j^z + s_i^z s_j^x)], \quad (1)$$

where $\gamma = X(Y)$ and $\alpha = Y(X)$ for the $x(y)$ bond, which reflects the bond-dependent K and Γ interactions, and ij refers to n.n. sites.

It is insightful to rewrite the above model in a global xyz coordinate system. In the ideal case, we take $\hat{y} = (1/\sqrt{2})[-110]$ which is parallel to the \hat{b} axis, and define $\hat{x} = (1/\sqrt{2})[110]$ to bisect the \hat{X} and \hat{Y} axis. Then, \hat{z} is fixed to the local oxygen direction $\hat{Z} = [001]$ as shown in Fig. 1(b). Transforming from XYZ to global xyz coordinates, the n.n. Hamiltonian is given by

$$H_{ij}^0 = J_K(s_i^x s_j^x + s_i^y s_j^y) + J s_i^z s_j^z + \frac{\Gamma}{\sqrt{2}}(s_i^x s_j^z + s_i^z s_j^x) + (-1)^i \left[-\frac{K}{2}(s_i^x s_j^y + s_i^y s_j^x) + \frac{\Gamma}{\sqrt{2}}(s_i^y s_j^z + s_i^z s_j^y) \right], \quad (2)$$

where $J_K = [J + (K/2)]$.

Before we present the strength of the J , K , and Γ interactions, let us discuss the impacts of K and Γ in the FM ordered state with $J < 0$. When $K < 0$, in the absence of Γ , $|J_K| > |J|$, the FM moment is within the xy plane, but pinned, via quantum fluctuations, towards the local \hat{X} or \hat{Y} axis along the oxygen directions. As we slightly turn on the AFM Γ interaction, the FM moment changes from the \hat{X} (or \hat{Y}) to \hat{x} axis, which makes an angle $\eta \sim 55^\circ$ from the $-\hat{c}$ axis. Upon increasing the AFM Γ strength, the moment stays in the $xz(ac)$ plane but tips closer towards the $-\hat{c}$ axis denoted by the red arrow $\mathbf{M}_{z'}$. Thus a reasonably sized AFM Γ interaction is required to achieve the moment direction consistent with experimental findings, $\eta \sim 31^\circ$ [2,4]. On the other hand, if the $K > 0$, in the absence of Γ , the FM moment is along the local Z axis denoted by the red arrow \mathbf{M}_z in Fig. 1(c), due to the AFM Kitaev term. This makes the angle of $\eta \sim 35^\circ$ from the $+\hat{c}$ direction, which is already close to experimental findings. Since Γ tips the moment away from the \hat{z} axis, it implies that $\Gamma \sim 0$ for $K > 0$.

The above analysis for ideal octahedral cages uncovers that the magnetic moment pinning direction is determined by either (i) AFM Kitaev or (ii) a combination of FM Kitaev and AFM Γ interactions. In solid-state materials such as CoNb_2O_6 , the octahedral lattice structure deviates from ideality. Octahedral distortions generate additional exchange interactions [35,37], which play a certain role in elucidating the phenomena observed in real materials. Presented below is the complete n.n. Hamiltonian formulation and the methodology employed to estimate these exchange interactions. Our focus is to identify the dominant interactions and determine the sign of the Kitaev interaction. This emphasis stems from the fact that the mechanism behind the Ising moment pinning hinges on the sign of K , which, in turn, gives information on the role of the Kitaev and Gamma interactions.

Hamiltonian with octahedra distortion—Octahedral distortions modify the ideal H_{ij}^0 and generates other bond-dependent interactions such as K' , Γ' , and Γ'' , see the Supplemental Material [39] for their definitions in the local XYZ coordinates. Among them K' needs some attention. While K takes the form of $s_i^x s_j^x$ for the x bond, K' takes the

form of $s_i^y s_j^y$ for the x bond (for y bond, they are $K s_i^y s_j^y$ and $K' s_i^x s_j^x$). Thus when $K = K'$, we lose the bond-dependent Kitaev interaction, and the model with $K = K'$ is nothing but the isotropic XY model. Similarly, when $\Gamma = \Gamma' = \Gamma''$, we lose the bond-dependent Γ interaction, and it maps to the XXZ model. In general, it requires a fine-tuning to make them equal.

In the global coordinates, with \hat{y} chosen to be parallel to the \hat{b} axis and \hat{x} chosen to bisect the local \hat{X} and \hat{Y}' axes making an angle 2θ , the n.n. Hamiltonian H_{ij} including the octahedra distortion has the following form:

$$H_{ij} = J_{xx} s_i^x s_j^x + J_{yy} s_i^y s_j^y + J_{zz} s_i^z s_j^z + J_{xz} (s_i^x s_j^z + s_i^z s_j^x) + (-1)^i [J_{xy} (s_i^x s_j^y + s_i^y s_j^x) + J_{yz} (s_i^y s_{i+1}^z + s_i^z s_{i+1}^y)], \quad (3)$$

where

$$\begin{aligned} J_{xx} &= \left(J + \frac{K + K'}{2} + \Gamma' \right) 2\cos^2(\theta), \\ J_{yy} &= \left(J + \frac{K + K'}{2} - \Gamma' \right) 2\sin^2(\theta), \quad J_{zz} = J, \\ J_{xz} &= (\Gamma + \Gamma'') \cos(\theta), \quad J_{yz} = (\Gamma - \Gamma'') \sin(\theta), \\ J_{xy} &= \frac{(K' - K)}{2} \sin(2\theta). \end{aligned} \quad (4)$$

The glide plane lies in the ac plane as shown in Fig. 1(a). Note that the exchange term $J s_i^z s_j^z$ is not modified by the distortion and its strength is determined by the Heisenberg interaction J . When $\theta = 45^\circ$, i.e., \hat{x} bisects \hat{X} and $\hat{Y}' = \hat{Y}'$, the above model is same as the ideal case, H_{ij}^0 [Eq. (2)]. In CoNb_2O_6 , $\theta \sim 40^\circ$ [4].

Let us now estimate the exchange parameters in Eq. (3). Because of the complexity of the exchange processes, it is challenging to pin down the numbers below 1 meV precisely using perturbation theory. Thus we are going to determine the dominant interactions using a combination of density function theory (DFT) and a strong coupling expansion up to the fourth order.

Determination of the exchange integrals—We estimate the hopping parameters, the crystal field splitting (Δ_c) and charge-transfer gap (Δ_{pd}) using DFT and maximally localized Wannier functions generated by OpenMX [40–43]. The strong coupling expansion requires determining all relevant hopping paths. For d^7 , there is one hole in t_{2g} and two holes in the e_g orbitals, resulting in three categories of exchange paths: $t_{2g} - t_{2g}$, $e_g - t_{2g}$, and $e_g - e_g$ processes, denoted as A , B , and C , respectively [25,37]. Each process further includes three different exchange mechanisms which are named intersite- U , charge transfer, and cyclic. Among them, the C process does not contribute to the Kitaev interaction, since $e_g - e_g$ exchanges do not change the angular momentum.

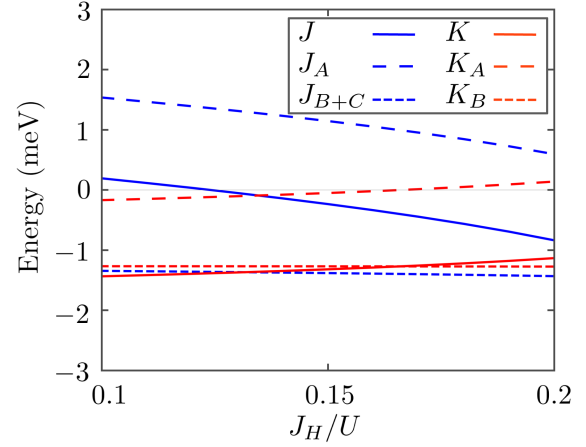


FIG. 2. The Heisenberg (blue) and Kitaev (red) interactions vs J_H/U for $\Delta_{pd}/U = 0.365$, $\Delta_c/U = 0.09$, and $U = 10$ eV. The contributions from $t_{2g} - t_{2g}$ (A), $t_{2g} - e_g$, and $e_g - e_g$ (B + C), and sum of A + B + C processes are represented by the dashed, dotted, and solid lines, respectively. See the main text for details.

After determining all relevant hopping parameters using DFT (see the Supplemental Material [39] for the tight binding parameters) and employing a strong coupling expansion, we find that the Kitaev and Heisenberg interactions are largest for a reasonable size of Hund's coupling as shown in Fig. 2. The dependence of J and K on the Hund's coupling strength in the range of $0.1 < J_H/U < 0.2$, suitable for cobalt ions [25], is shown in Fig. 2 where the A, B, and C processes are plotted using different line styles. The red and blue lines represent the Kitaev and Heisenberg interactions, respectively. The solid lines are the total Kitaev and Heisenberg interactions after summing A, B, and C processes; overall, we find that both interactions are FM.

For $J_H/U = 0.2$, the two dominant interactions are $J = -0.8$ and $K = -1.1$ meV. We estimate the remaining exchange integrals by computing the DSF from exact diagonalization (ED), using the open-source numerical package QuSpin [44], and fit it with the INS data [14] as shown in Fig. 3. The details about the DSF computation and systematic fitting procedure to the INS data are explained in the Supplemental Material [39]. A summary of the n.n. exchange parameters is listed in Table I and the mapping to $J_{\alpha,\beta}$ with $\alpha, \beta = x, y, z$ is also listed. Note that the $K < 0$ and $J < 0$, while $\Gamma > 0$. The significant values of J_{xy} and J_{xz} highlight the importance of K and Γ , as indicated by their relationships in Eq. (4). With the parameter set listed in Table I, we found that the Ising moment aligns along the \mathbf{M}_z direction with $\eta \sim 35^\circ$ due to the sizable AFM Γ interaction, which causes the moment direction to deviate from the \hat{x} axis towards the $-\hat{c}$ axis, as illustrated by the blue arrow in Fig. 1(c).

It is important to note that the Kitaev interaction stays FM and dominant. This is due to an AFM exchange contribution from $t_{2g} - t_{2g}$ processes which cancels with the FM contribution from $e_g - t_{2g}$ and $e_g - e_g$ processes,

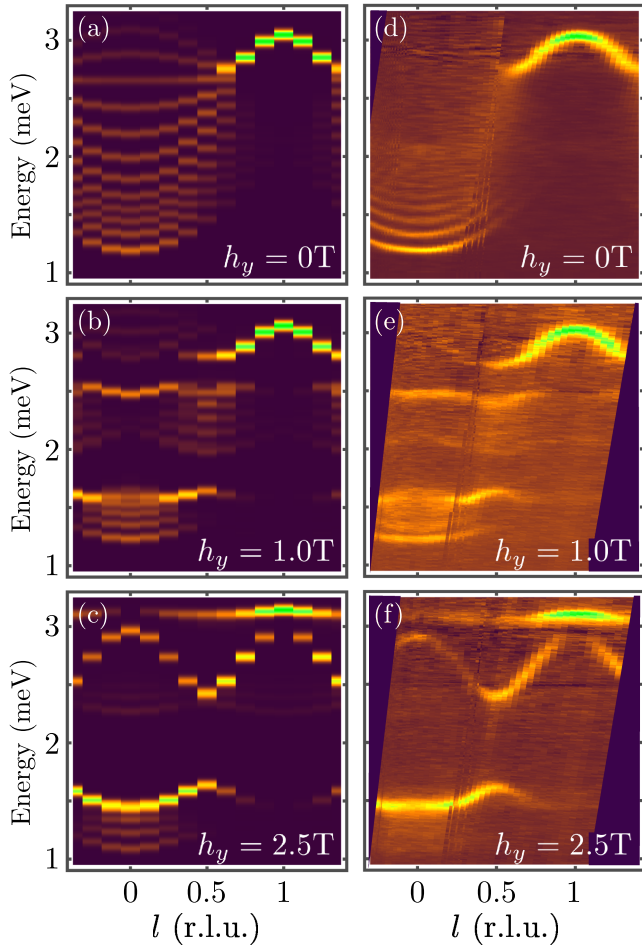


FIG. 3. (a)–(c) $S^{xx}(k, w)$ at various transverse fields obtained by the ED on a 16-site cluster with periodic boundary conditions using the parameters summarized in Table I with second n.n. XXZ interactions, a small mean field term, and $g_y = 3.3$ (see the main text for details). (d)–(f) The INS data are adopted from Ref. [14]. The details of the INS calculations are provided in the Supplemental Material [39].

resulting in a small FM J . This can be contrasted with $3d^7$ honeycomb cobaltates, such as $\text{BaCo}_2(\text{AsO}_4)_2$ which has a much larger direct hopping integral leading to the cancellation of Kitaev contribution from $t_{2g} - t_{2g}$ and $t_{2g} - e_g$

TABLE I. Strengths of spin-1/2 n.n. exchange interactions in local XYZ coordinates, and their transformed values in global xyz coordinates.

Interaction in (XYZ)	meV	Interaction in (xyz)	meV
J	−0.8	J_{xx}	−2.27
K	−1.1	J_{yy}	−0.66
Γ	0.56	$J_{zz} = J$	−0.80
K'	−0.03	J_{xy}	0.53
Γ'	−0.57	J_{xz}	0.63
Γ''	0.26	J_{yz}	0.19

processes yielding a small Kitaev interaction, but dominant FM Heisenberg interaction [37]. The Kitaev interaction becomes more dominant by moving towards the Mott insulating limit; increasing the charge-transfer gap (Δ_{pd}) while keeping the Hubbard U fixed results in a faster reduction of the FM Heisenberg interaction strength due to a larger AFM contribution from the $t_{2g} - t_{2g}$ processes (see the Supplemental Material).

Significance of the sign of the Kitaev interaction—Our theory offers two ways to generate Ising behavior. Interestingly, the Ising axis as the moment direction consistent with the experimental results in CoNb_2O_6 also presents two distinct possibilities: aligning the Ising axis either with \mathbf{M}_z or $\mathbf{M}_{z'}$, as depicted by the red arrows in Fig. 1(c). Let us investigate microscopic origins of the two possibilities and their implications.

Imagine that the moment aligns with the z axis, directed towards the oxygen atom, which aligns with INS data when the dominant FM J condition holds ($|J|(\equiv |J_{zz}|) > |J_{xx}|, |J_{yy}|$). This condition necessitates a significant AFM Kitaev but minimal Γ interactions, enforcing $J_{xy} = 0$ and $J_{xz} = 0$ as noted in [10,14,45]. Consequently, $K = K'$ and $\Gamma = -\Gamma''$. This, combined with the J term, yields the FM XXZ model with pronounced Ising anisotropy along the local Z axis, i.e., traditional XXZ magnets. However, from a microscopic viewpoint presented above, the equality $K = K'$ is unlikely due to the need for identical contributions from the exchange path of $d_{xz}-d_{xy}$ and $d_{yz}-d_{xy}$ orbitals for a given bond. Furthermore, the Kitaev interaction is FM.

Alternatively, aligning the Ising axis along $\mathbf{M}_{z'}$ away from the oxygen atom, as found in our theory, offers another approach. This is a nontraditional Ising magnet, as the pinning of moment is due to the bond-dependent AFM Gamma interaction in the presence of FM Kitaev interaction, which cannot be reduced to the standard anisotropic XXZ type. Furthermore, adopting this z' axis as the empirical Ising axis allows for the transformation of parameters outlined in Table I in the xyz to $x'y'z'$ coordinates while keeping $\hat{y} = \hat{y}'$. The comparison between exchange interactions in $x'y'z'$ coordinates and xyz coordinates is provided in the Supplemental Material [39]. The resulting n.n. interactions in $x'y'z'$ coordinates remarkably resembles those reported in [10,14,45], further corroborating our results.

Discussion and summary—Our theory provides a microscopic origin of Ising behaviors in spin-orbit coupled chains beyond the example of CoNb_2O_6 presented here. It extends beyond the symmetry-allowed spin model and differs from other analyses [10,14,45–47], where the Ising axis is empirically chosen, which impedes the identification of the origin of the Ising anisotropy.

To advance research on two-dimensional Kitaev cobaltates, it is noteworthy to observe the distinction between

CoNb₂O₆ and honeycomb cobaltates such as BaCo₂(AsO₄)₂, where the Kitaev interaction is weakened due to exchange path cancellation [37]. This difference is primarily linked to cobalt ion spacing. Our study suggests that increasing the Co-Co distance to minimize direct exchange is advantageous for enhancing the Kitaev interaction in honeycomb cobaltates, thus facilitating the realization of the Kitaev spin liquid.

In summary, through an examination of the exchange interactions derived from the $J_{\text{eff}} = 1/2$ wave functions in the local oxygen coordinates, we show that the Ising anisotropy arises from an AFM Γ interaction in the presence of a FM Kitaev interaction, which also facilitates domain wall motion. Our theory illustrates that CoNb₂O₆, once considered an Ising chain exemplar, is a rare bond-dependent Kitaev chain, where the Kitaev interaction predominates. Our theory offers an alternative angle on Ising behaviors in 1D Ising systems and will motivate future investigations into various Ising-like chains.

Acknowledgments—We thank P. Armitage, R. Coldea, X. Liu, and L. Woodland for useful discussions. This work is supported by the NSERC Discovery Grant No. 2022-04601. H. Y. K. acknowledges support from the Canada Research Chairs Program. Computations were performed on the Niagara supercomputer at the SciNet HPC Consortium. SciNet is funded by the Canada Foundation for Innovation under the auspices of Compute Canada, the Government of Ontario, Ontario Research Fund—Research Excellence, and the University of Toronto.

-
- [1] I. Maartense, I. Yaeger, and B. Wanklyn, *Solid State Commun.* **21**, 93 (1977).
- [2] W. Scharf, H. Weitzel, I. Yaeger, I. Maartense, and B. Wanklyn, *J. Magn. Magn. Mater.* **13**, 121 (1979).
- [3] T. Hanawa, K. Shinkawa, M. Ishikawa, K. Miyatani, K. Saito, and K. Kohn, *J. Phys. Soc. Jpn.* **63**, 2706 (1994).
- [4] C. Heid, H. Weitzel, P. Burlet, M. Bonnet, W. Gonschorek, T. Vogt, J. Norwig, and H. Fuess, *J. Magn. Magn. Mater.* **151**, 123 (1995).
- [5] I. Cabrera, J. D. Thompson, R. Coldea, D. Prabhakaran, R. I. Bewley, T. Guidi, J. A. Rodriguez-Rivera, and C. Stock, *Phys. Rev. B* **90**, 014418 (2014).
- [6] R. Coldea, D. A. Tennant, E. M. Wheeler, E. Wawrzynska, D. Prabhakaran, M. Telling, K. Habicht, P. Smeibidl, and K. Kiefer, *Science* **327**, 177 (2010).
- [7] S. B. Rutkevich, *J. Stat. Mech.* (2010) P07015.
- [8] J. A. Kjall, F. Pollmann, and J. E. Moore, *Phys. Rev. B* **83**, 020407(R) (2011).
- [9] M. Nandi, D. Prabhakaran, and P. Mandal, *J. Phys. Condens. Matter* **31**, 195802 (2019).
- [10] M. Fava, R. Coldea, and S. A. Parameswaran, *Proc. Natl. Acad. Sci. U.S.A.* **117**, 25219 (2020).
- [11] Y. Xu, L. S. Wang, Y. Y. Huang, J. M. Ni, C. C. Zhao, Y. F. Dai, B. Y. Pan, X. C. Hong, P. Chauhan, S. M. Koohpayeh, N. P. Armitage, and S. Y. Li, *Phys. Rev. X* **12**, 021020 (2022).
- [12] J. A. Ringler, A. I. Kolesnikov, and K. A. Ross, *Phys. Rev. B* **105**, 224421 (2022).
- [13] J. Park, S. H. Lee, S. Bae, M. H. Kim, and S. Yoon, *Cryst. Growth Des.* **23**, 4395 (2023).
- [14] L. Woodland, I. Lovas, M. Telling, D. Prabhakaran, L. Balents, and R. Coldea, *Phys. Rev. B* **108**, 184417 (2023).
- [15] T. Liang, S. M. Koohpayeh, J. W. Krizan, T. M. McQueen, R. J. Cava, and N. P. Ong, *Nat. Commun.* **6**, 7611 (2015).
- [16] C. M. Morris, R. Valdés Aguilar, A. Ghosh, S. M. Koohpayeh, J. Krizan, R. J. Cava, O. Tchernyshyov, T. M. McQueen, and N. P. Armitage, *Phys. Rev. Lett.* **112**, 137403 (2014).
- [17] K. Amelin, J. Engelmayer, J. Viirok, U. Nagel, T. Room, T. Lorenz, and Z. Wang, *Phys. Rev. B* **102**, 104431 (2020).
- [18] C. M. Morris, N. Desai, J. Viirok, D. Hüvonen, U. Nagel, T. Rõõm, J. W. Krizan, R. J. Cava, T. M. McQueen, S. M. Koohpayeh, R. K. Kaul, and N. P. Armitage, *Nat. Phys.* **17**, 832 (2021).
- [19] K. Amelin, J. Viirok, U. Nagel, T. Rõõm, J. Engelmayer, T. Dey, A. A. Nugroho, T. Lorenz, and Z. Wang, *J. Phys. A* **55**, 484005 (2022).
- [20] A. W. Kinross, M. Fu, T. J. Munsie, H. A. Dabkowska, G. M. Luke, S. Sachdev, and T. Imai, *Phys. Rev. X* **4**, 031008 (2014).
- [21] B. M. McCoy and T. T. Wu, *Phys. Rev. D* **18**, 1259 (1978).
- [22] A. B. Zamolodchikov, *Int. J. Mod. Phys. A* **04**, 4235 (1989).
- [23] G. Delfino, G. Mussardo, and P. Simonetti, *Nucl. Phys. B* **473**, 469 (1996).
- [24] S. B. Rutkevich, *J. Stat. Phys.* **131**, 917 (2008).
- [25] H. Liu and G. Khaliullin, *Phys. Rev. B* **97**, 014407 (2018).
- [26] R. Sano, Y. Kato, and Y. Motome, *Phys. Rev. B* **97**, 014408 (2018).
- [27] G. Khaliullin, *Prog. Theor. Phys. Suppl.* **160**, 155 (2005).
- [28] A. Kitaev, *Ann. Phys. (Amsterdam)* **321**, 2 (2006).
- [29] G. Jackeli and G. Khaliullin, *Phys. Rev. Lett.* **102**, 017205 (2009).
- [30] J. c. v. Chaloupka, G. Jackeli, and G. Khaliullin, *Phys. Rev. Lett.* **105**, 027204 (2010).
- [31] J. G. Rau, E. K.-H. Lee, and H.-Y. Kee, *Phys. Rev. Lett.* **112**, 077204 (2014).
- [32] J. G. Rau, E. K.-H. Lee, and H.-Y. Kee, *Annu. Rev. Condens. Matter Phys.* **7**, 195 (2016).
- [33] S. M. Winter, A. A. Tsirlin, M. Daghofer, J. van den Brink, Y. Singh, P. Gegenwart, and R. Valentí, *J. Phys. Condens. Matter* **29**, 493002 (2017).
- [34] Y. Motome, R. Sano, S. Jang, Y. Sugita, and Y. Kato, *J. Phys. Condens. Matter* **32**, 404001 (2020).
- [35] H. Liu, J. c. v. Chaloupka, and G. Khaliullin, *Phys. Rev. Lett.* **125**, 047201 (2020).
- [36] S. M. Winter, *J. Phys.* **5**, 045003 (2022).
- [37] X. Liu and H.-Y. Kee, *Phys. Rev. B* **107**, 054420 (2023).
- [38] I. Rousochatzakis, N. Perkins, Q. Luo, and H.-Y. Kee, *Rep. Prog. Phys.* **87**, 026502 (2024).

- [39] See Supplemental Material at <http://link.aps.org/supplemental/10.1103/PhysRevLett.133.056703> for tight binding parameters obtained by the density functional theory, strong-coupling expansion, spin models in different coordinates, and dynamical structure factors with various parameter sets.
- [40] T. Ozaki, *Phys. Rev. B* **67**, 155108 (2003).
- [41] T. Ozaki and H. Kino, *Phys. Rev. B* **69**, 195113 (2004).
- [42] T. Ozaki and H. Kino, *Phys. Rev. B* **72**, 045121 (2005).
- [43] K. Lejaeghere *et al.*, *Science* **351**, aad3000 (2016).
- [44] P. Weinberg and M. Bukov, *SciPost Phys.* **7**, 020 (2019).
- [45] L. Woodland, D. Macdougall, I.M. Cabrera, J.D. Thompson, D. Prabhakaran, R.I. Bewley, and R. Coldea, *Phys. Rev. B* **108**, 184416 (2023).
- [46] C. A. Gallegos and A. L. Chernyshev, *Phys. Rev. B* **109**, 014424 (2024).
- [47] A. A. Konieczna, D. A. S. Kaib, S. M. Winter, and R. Valenti, [arXiv:2406.17854](https://arxiv.org/abs/2406.17854).